BOUT++ 2023 Workshop
Hertz Hall, Livermore, USA, 2023-01-09

A BOUT++ Extension for Full Annular Tokamak Edge MHD and Turbulence Simulations

H. Seto (QST)

In collaboration with

B.D. Dudson (LLNL), X.Q. Xu (LLNL), M. Yagi (QST)

This work is published as Seto et al., Comput Phys. Commun. **283** (2023) 108568

Acknowledgement:

This work was partly supported by JSPS KAKENHI Grant No. 20K14448 and performed under EU-Japan BA collaboration, under JIFT collaboration between QST and LLNL and under the auspices of U.S. Department of Energy by LLNL under Contract No. DE-AC52-07NA27344. The computations were carried out on JFRS-1 supercomputer at IFERC-CSC and on SGI HPE8600 supercomputer at QST and JAEA.

Outline

- Introduction

- BOUT++ coordinate systems and hybrid field solver developed for full annular tokamak edge simulation

- Pedestal collapse with resistive drift-ballooning mode (RDBM) turbulence in shifted circular domain

  - ➢ Scan of the maximum toroidal mode number solved by 2D field solver against pedestal collapse

  - ➢ Impact of truncated toroidal domain on energy loss process

  - ➢ Nonlinear generation on=1 global mode during pedestal collapse

- Summary

Low-n is an issue for full torus nonlinear simulation in BOUT++

BOUT++ as a tokamak edge simulation code [Dudson+ CPC'09]

- Moderate- (O(n)>1) and high-n (O(n)≫1) modes can be with high accuracy by dual coordinate system (field-aligned coordinates & flux-surface coordinates)
  - ➢ Field solver for flow potential is reduced to 1D problem with flute-ordering

- Low-n (O(n)~1) modes sometimes suffer numerical instability due to the usage of flute-ordering $k_{//}=0$ in the field solver calculating flow potential
  - ➢ Computational domain can be limited to wedge torus for numerical instability as well as for saving computational cost

Low-n is an issue for full torus nonlinear simulation in BOUT++

BOUT++ as a tokamak edge simulation code [Dudson+ CPC'09]

- Moderate- (O(n)>1) and high-n (O(n)≫1) modes can be with high accuracy with dual coordinate system (field-aligned coordinates & flux-surface coordinates)
  - ➢ Field solver for flow potential is reduced to 1D problem with flute-ordering

- Low-n (O(n)~1) modes sometimes suffer numerical instability due to the usage of flute-ordering $k_{//}=0$ in the field solver calculating flow potential
  - ➢ Computational domain can be limited to wedge torus for numerical instability as well as for saving computational cost

➡ Improving low-n modes (taking full annular torus domain) is a key for more reliable tokamak edge simulations

- Convergence of core ITG turbulence against wedge number [K. Kim PoP2017]
- Nonlinear stabilization of ELM by muti-mode interaction [P.W. Xi PRL2014]

Large wedge number *N* can result in "false convergence" in core ITG turbulence [by XGC1, K. Kim PoP2017]

Fig. 7 in K. Kim et al, Phys. Plasmas 24, 012306 (2017)

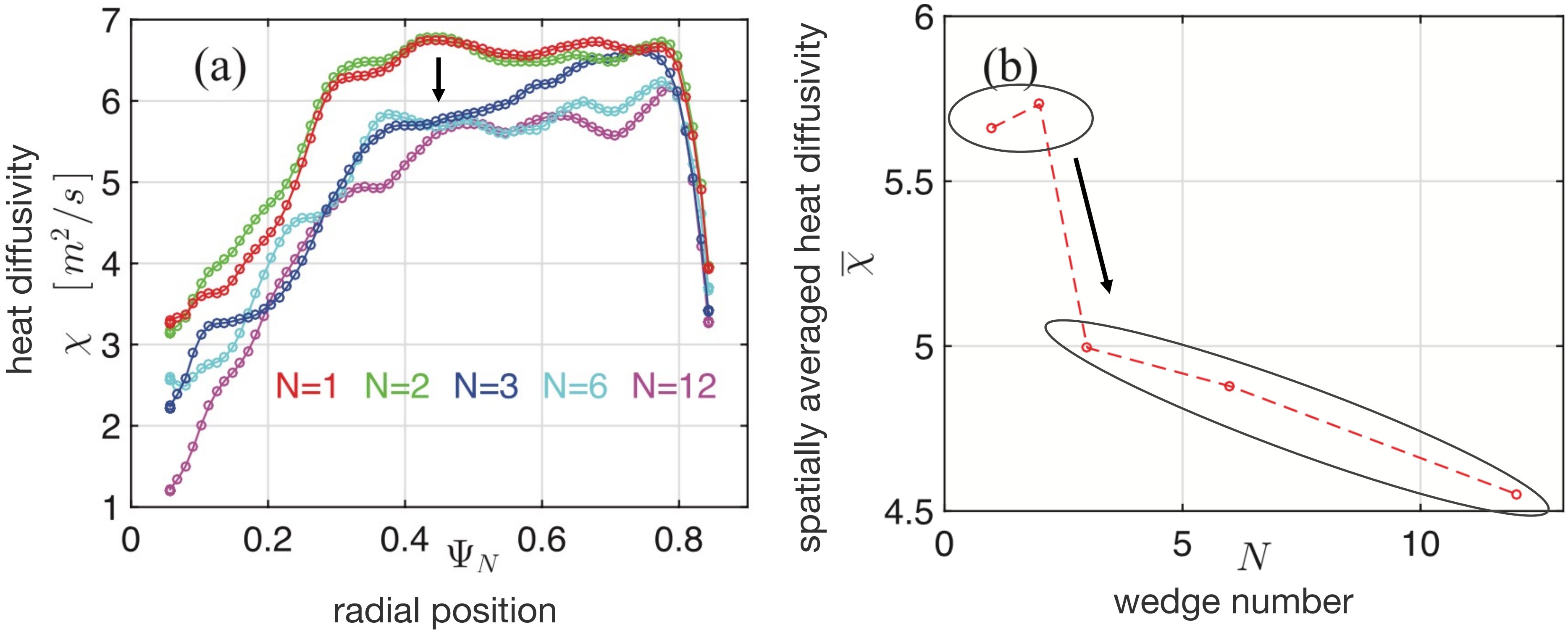

Full-f core ITG turbulence simulations with different wedge numbers *N* (1/*N* wedge tori)

- non-negligible heat transport reduction between N=2 and N=3
- Convergence study in wedge number is needed to avoid "false convergence"

➡ Convergence study in wedge number can be also important for edge turbulence

Nonlinear stabilization effect by mode-mode coupling can change ELM crash criteria [by BOUT++, P.W. Xi PRL2014]

Fig. 1 in P.W. Xi et al, Phys. Rev. Lett 112 (2014) 085001

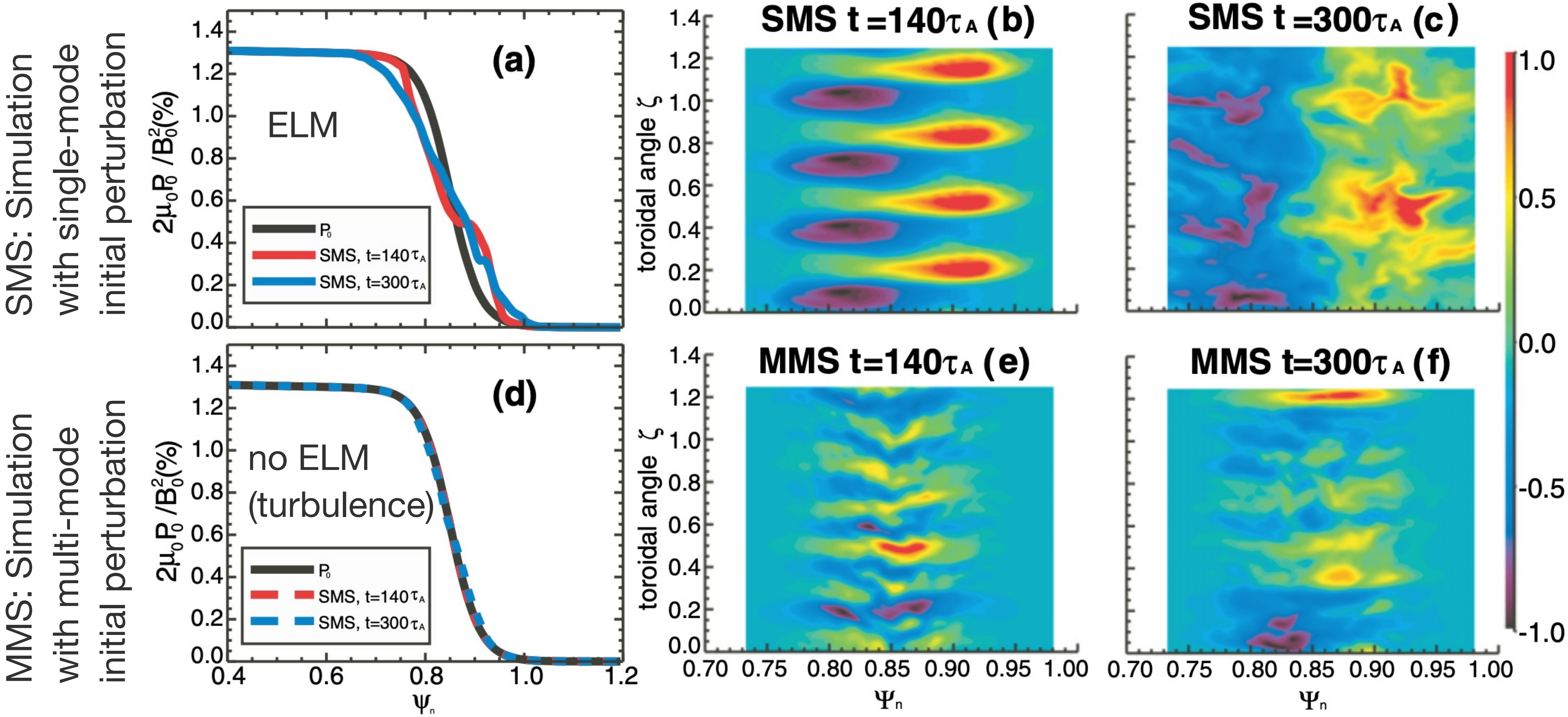

Simulation with multi-mode initial perturbations and with single mode perturbation in 1/5th annular wedge torus captures the bifurcation between ELM and turbulence

➡ Full torus run is needed to handle complete set of nonlinear mode-mode couplings

Objective of this work

BOUT++ framework is extended with a hybrid field solver to address to full annular tokamak edge simulations, which is a key for

- Current-driven (low-n) giant ELMs
- ELM control by RMPs, edge turbulence with RMPs
- Convergence study against the wedge number for edge turbulence
- ELM crash with interplay between n=0 flow, low-n MHD and high-n turbulence

Outline

- Introduction
- BOUT++ coordinate systems and hybrid field solver developed for full annular tokamak edge simulation
- Pedestal collapse with resistive drift-ballooning mode (RDBM) turbulence in shifted circular domain
  - ➢ Scan of the maximum toroidal mode number solved by 2D field solver against pedestal collapse
  - ➢ Impact of truncated toroidal domain on energy loss process
  - ➢ Nonlinear generation on=1 global mode during pedestal collapse
- Summary

Low-n field solver is discretized in flux surface coordinates

2D Helmholtz Eq. for toroidal mode n defined in flux surface coords. (ψ,θ,ζ)

$$\left(d\nabla_\perp^2 + \frac{1}{c}\nabla c\cdot\nabla_\perp + a\right) f(x,y,z) = h(x,y,z)$$

(x,y,z): field-aligned coordinates

(ψ,θ,ζ): flux-surface coordinates

coordinate transform in Fourier space

$$d\left[L_{\mathrm{fs}}^{10}\frac{\partial}{\partial\psi} + L_{\mathrm{fs}}^{11}\frac{\partial^2}{\partial\psi^2} + \left(L_{\mathrm{fs}}^{20} + inL_{\mathrm{fs}}^{23}\right)\frac{\partial}{\partial\theta} + L_{\mathrm{fs}}^{22}\frac{\partial}{\partial\theta^2} + inL_{\mathrm{fs}}^{30} - n^2L_{\mathrm{fs}}^{33}\right]F(\psi,\theta|n)$$
$$+\frac{1}{c}\left(G_{\mathrm{fs}}^{1}\frac{\partial c}{\partial\psi}\frac{\partial}{\partial\psi} + G_{\mathrm{fs}}^{2}\frac{\partial c}{\partial\theta}\frac{\partial}{\partial\theta} + inG_{\mathrm{fs}}^{3}\frac{\partial c}{\partial\theta}\right)F(\psi,\theta|n) + aF(\psi,\theta|n) = H(\psi,\theta|n)$$

Low-n field solver is discretized in flux surface coordinates

2D Helmholtz Eq. for toroidal mode n defined in flux surface coords. (ψ,θ,ζ)

(x,y,z): field-aligned coordinates

(ψ,θ,ζ): flux-surface coordinates

$$\left(d\nabla_\perp^2 + \frac{1}{c}\nabla c \cdot \nabla_\perp + a\right) f\underline{(x,y,z)} = h\underline{(x,y,z)}$$

coordinate transform in Fourier space

$$d\left[L_{\text{fs}}^{10}\underline{\frac{\partial}{\partial\psi}} + L_{\text{fs}}^{11}\underline{\frac{\partial^2}{\partial\psi^2}} + \left(L_{\text{fs}}^{20} + inL_{\text{fs}}^{23}\right)\underline{\frac{\partial}{\partial\theta}} + L_{\text{fs}}^{22}\underline{\frac{\partial}{\partial\theta^2}} + inL_{\text{fs}}^{30} - n^2L_{\text{fs}}^{33}\right]F(\underline{\psi,\theta}|n)$$
$$+\frac{1}{c}\left(G_{\text{fs}}^{1}\frac{\partial c}{\partial\psi}\underline{\frac{\partial}{\partial\psi}} + G_{\text{fs}}^{2}\frac{\partial c}{\partial\theta}\underline{\frac{\partial}{\partial\theta}} + inG_{\text{fs}}^{3}\frac{\partial c}{\partial\theta}\right)F(\underline{\psi,\theta}|n) + aF(\underline{\psi,\theta}|n) = H(\underline{\psi,\theta}|n)$$

- Discretized with 4th order central differences on (ψ,θ)-plane and solved iteratively by GMRES + AMG precondition with PETSc and Hypre libraries
  - ➢ Problem size: one matrix of O($N_\psi * N_\theta$) rather than N_y matrices of O(N_ψ)
  - ➢ Slower than the flute-ordered solver but more stable for low-n modes

Low-n field solver is discretized in flux surface coordinates

2D Helmholtz Eq. for toroidal mode n defined in flux surface coords. (ψ,θ,ζ)

(x,y,z): field-aligned coordinates

(ψ,θ,ζ): flux-surface coordinates

$$\left(d\nabla_\perp^2 + \frac{1}{c}\nabla c\cdot\nabla_\perp + a\right) f(x,y,z) = h(x,y,z)$$

coordinate transform in Fourier space

$$d\left[L_{\rm fs}^{10}\frac{\partial}{\partial\psi} + L_{\rm fs}^{11}\frac{\partial^2}{\partial\psi^2} + \left(L_{\rm fs}^{20} + inL_{\rm fs}^{23}\right)\frac{\partial}{\partial\theta} + L_{\rm fs}^{22}\frac{\partial}{\partial\theta^2} + inL_{\rm fs}^{30} - n^2L_{\rm fs}^{33}\right]F(\psi,\theta|n)$$
$$+\frac{1}{c}\left(G_{\rm fs}^{1}\frac{\partial c}{\partial\psi}\frac{\partial}{\partial\psi} + G_{\rm fs}^{2}\frac{\partial c}{\partial\theta}\frac{\partial}{\partial\theta} + inG_{\rm fs}^{3}\frac{\partial c}{\partial\theta}\right)F(\psi,\theta|n) + aF(\psi,\theta|n) = H(\psi,\theta|n)$$

- Discretized with 4th order central differences on (ψ,θ)-plane and solved iteratively by GMRES + AMG precondition with PETSc and Hypre libraries
  - ➢ Problem size: one matrix of O($N_\psi * N_\theta$) rather than N_y matrices of O(N_ψ)
  - ➢ Slower than the flute-ordered solver but more stable for low-n modes
- The number of poloidal grids N_θ should be same as that of parallel grids N_y for transform between field-aligned (x,y,z) and flux surface (ψ,θ,ζ) coordinates
  - ➢ Poloidal resolution be fine enough for resonant poloidal modes $m_{\rm res}=nq$
  - ➢ Hybrid field solver (low-n: 2D solver + high-n: 1D solver) is reasonable from the viewpoint of computational cost

A hybrid field solver for full annular tokamak edge simulation

field-aligned coordinates | flux-surface coordinates (Fourier space)

$$x = \psi - \psi_0$$
$$y = \theta$$
$$z = \zeta - \alpha$$
$$\alpha = \int_{\theta_0}^{\theta} \frac{B^\zeta}{B^\theta} d\theta$$

Inputs

① $h(x, y, z)$

FFT & Phase shift: $\zeta = z + \alpha$

② $H(\psi, \theta, n)$

③ 2D field solver for $0 \leq n \leq n_{\mathrm{2Dmax}}$

$$F(\psi, \theta | n) = \mathcal{L}_{\mathrm{2D}}^{-1} H(\psi, \theta | n)$$

1D field solver for $n_{\mathrm{2Dmax}} < n \leq n_{\mathrm{1Dmax}}$

$$F(\psi | \theta, n) = \mathcal{L}_{\mathrm{1D}}^{-1} H(\psi | \theta, n)$$

④ $$F(\psi, \theta, n) = \sum_{n'=0}^{n_{\mathrm{2Dmax}}} F(\psi, \theta | n') + \sum_{n'=n_{\mathrm{2Dmax}+1}}^{n_{\mathrm{1Dmax}}} F(\psi | \theta, n')$$

Phase shift & FFT: $z = \zeta - \alpha$

Output

⑤ $f(x, y, z)$

The maximum toroidal mode number solved by 2D field solver n_{2Dmax} is a free parameter and should be chosen carefully not to affect simulation result

Outline

- Introduction
- BOUT++ coordinate systems and hybrid field solver developed for full annular tokamak edge simulation
- Pedestal collapse with resistive drift-ballooning mode (RDBM) turbulence in full annular torus with shifted circular cross section
  - Scan of the maximum toroidal mode number solved by 2D field solver against pedestal collapse
  - Impact of truncated toroidal domain on energy loss process
  - Nonlinear generation on=1 global mode during pedestal collapse
- Summary

Simulation setup for pedestal collapse simulation

- **IBM marginally unstable shifted circular equilibrium (R_{ax}=3.5m, B_{ax}=2T)**

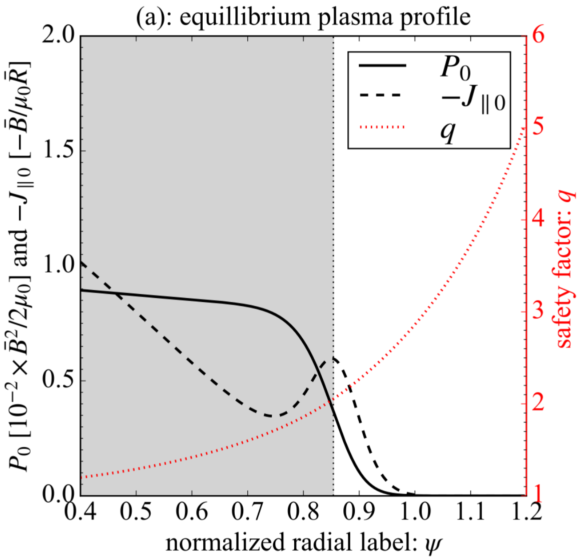

➢ **Energy loss level**

$$\Delta W_{\rm ped}/W_{\rm ped} = -\int_{V_{\rm ped}} P_1 dV / \int_{V_{\rm ped}} P_0 dV,$$

V_{ped} is the volume inside the ∇P_0 peak (shaded region)

➢ **Perpendicular kinetic energy**

$$W_{\rm kin}(n') = -\frac{1}{V_{\rm all}}\int_{V_{\rm all}} F^{n=n'}\varpi dV = \frac{1}{V_{\rm all}}\int_{V_{\rm all}} \frac{|\nabla_\perp F^{n=n'}|^2}{2B_0^2} dV,$$

V_{all} is the whole simulated domain

- **Scale separated 4-field RDBM model [Seto+ CPP'20]**

$$\frac{\partial}{\partial t}\varpi_1 = -[F_1,\varpi] - [F_0,\varpi_1] + \mathcal{G}(p_1,F) + \mathcal{G}(p_0,F_1) - B_0\partial_\parallel\left(\frac{J_{\parallel 1}}{B_0}\right) + B_0\left[A_{\parallel 1},\frac{J_\parallel}{B_0}\right] + \mathcal{K}(p_1) + \mu_\parallel\partial_\parallel^2\varpi_1 + \mu_\perp\nabla_\perp^2\varpi_1,$$

$$\frac{\partial}{\partial t}p_1 = -[\phi_1,p] - [\phi_0,p_1] - 2\beta_*\left(\mathcal{K}(p_1) - B_0\partial_\parallel\left(\frac{v_{\parallel 1}+d_iJ_{\parallel 1}}{2B_0}\right) + B_0\left[A_{\parallel 1},\frac{v_{\parallel 1}+d_iJ_{\parallel 1}}{2B_0}\right]\right) + \chi_\parallel\partial_\parallel^2 p_1 + \chi_\perp\nabla_\perp^2 p_1,$$

$$\frac{\partial}{\partial t}A_{\parallel 1} = -[\phi,A_{\parallel 1}] - \partial_\parallel\phi_1 + \delta_e\left(\partial_\parallel p_1 - [A_{\parallel 1},p]\right) + \eta J_{\parallel 1} - \lambda\nabla_\perp^2 J_{\parallel 1},$$

$$\frac{\partial}{\partial t}v_{\parallel 1} = -[\phi,v_{\parallel 1}] - \frac{1}{2}\left(\partial_\parallel p_1 - [A_{\parallel 1},p]\right) + \nu_\perp\nabla_\perp^2 v_{\parallel 1},$$

$$\varpi = \nabla_\perp^{*2}F,\quad J_1 = \nabla_\perp^2 A_\parallel,\quad F = \phi + \delta_i p,\quad \phi = \phi_0 + \phi_1,\quad p = p_0 + p_1,\quad \boldsymbol{B} = \boldsymbol{B}_0 + \nabla A_{\parallel 1}\times\boldsymbol{b}_0,\quad J_\parallel = J_{\parallel 0} + J_{\parallel 1},$$

$$n_{i0} = 10^{19}\ [m^{-3}],\quad \eta = 10^{-8},\quad \lambda = 10^{-12},\quad \mu_\perp = \chi_\perp = \nu_\perp = 10^{-7},\quad \mu_\parallel = \chi_\parallel = 10^{-1}$$

➢ Initially most unstable toroidal mode: n=32

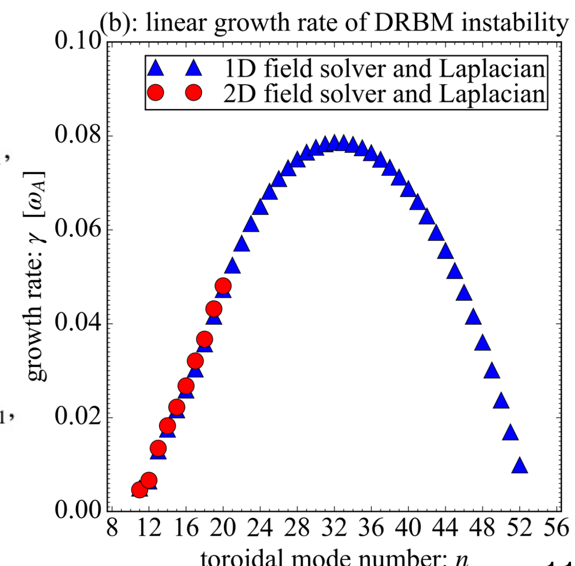

Sensitivity scan of n2Dmax against full annular torus pedestal collapse simulation

3 runs with different n_{2Dmax} =4, 8, 12 with Nx=516, Ny=256, Nz=256, n_{1Dmax}=80

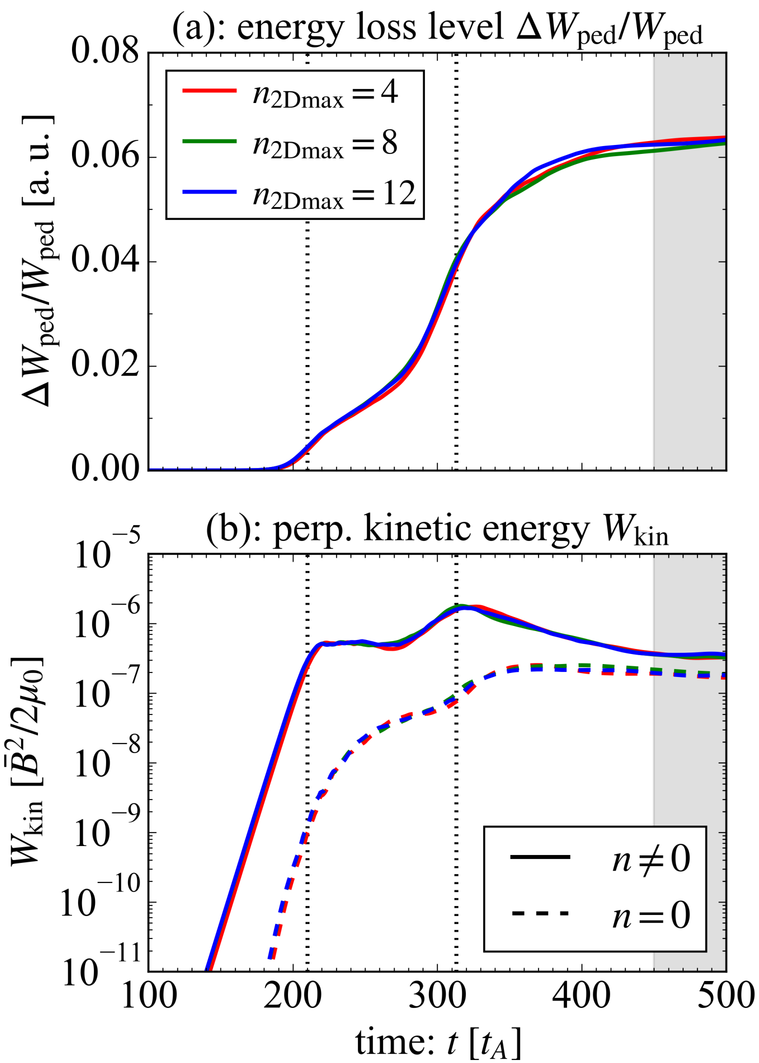

Sensitivity scan of n2Dmax against full annular torus pedestal collapse simulation

3 runs with different n_{2Dmax} = 4, 8, 12 (Nx=516, Ny=256, Nz=256, n_{1Dmax}=80)

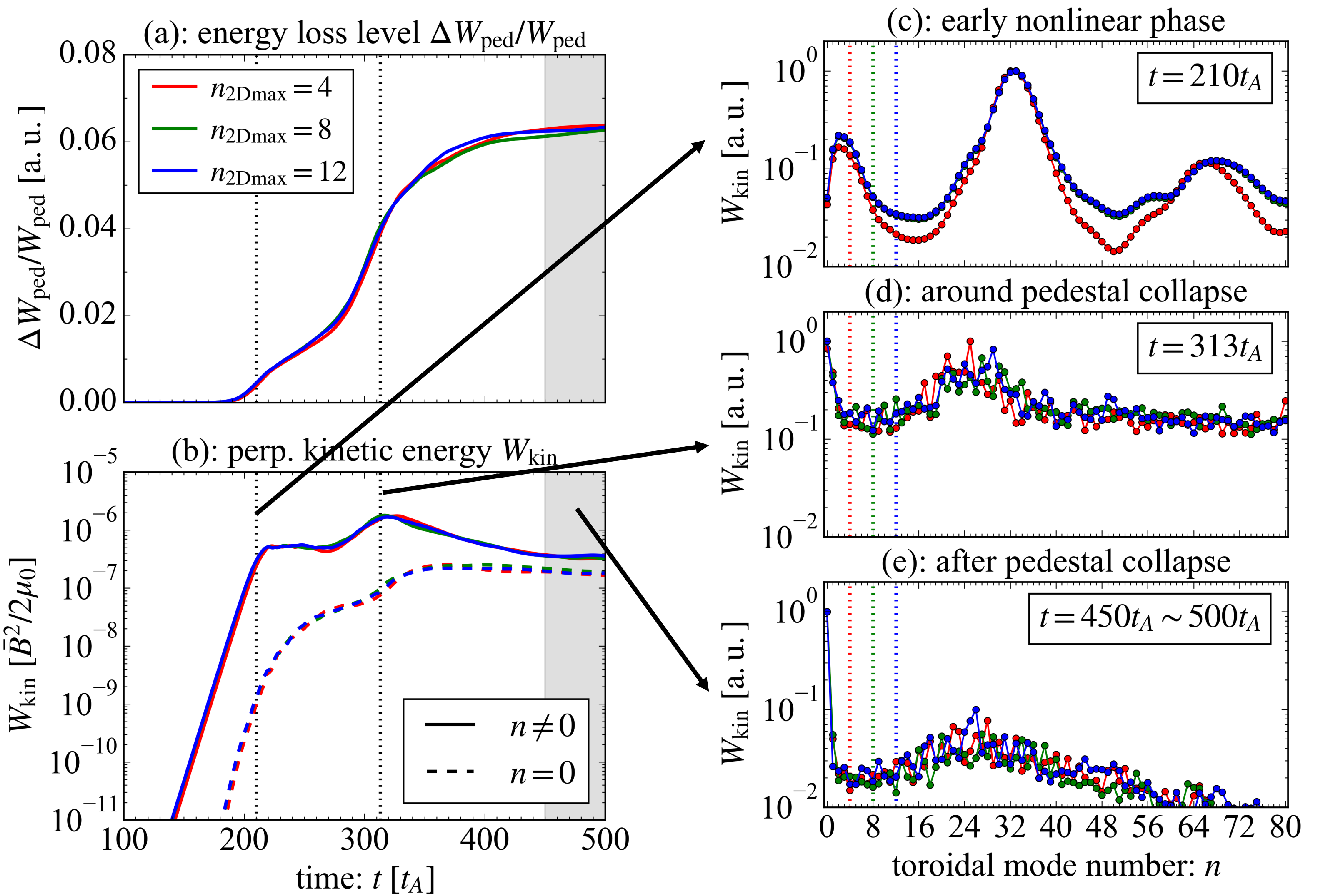

n_{2Dmax} =4 is high enough in this simulation setup

Toroidal domain length qualitatively changes energy loss process during pedestal collapse

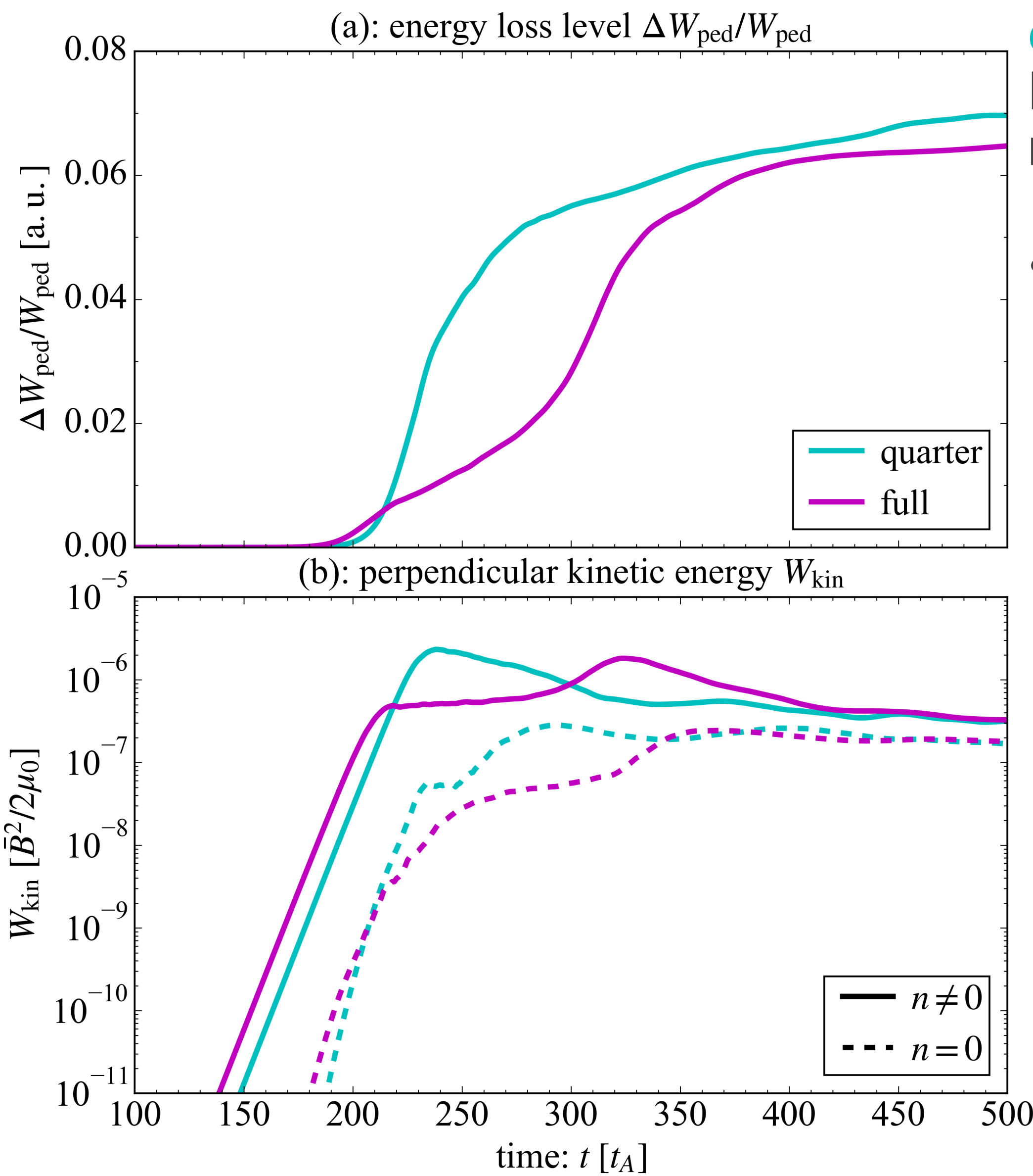

quarter and full toru run with Nx=1028, Ny=128, Nz= 64 or 256, n_{2Dmax}=4, n_{1Dmax}=80

- Resultant energy loss and n=0 and n≠0 amplitude of kinetic energy saturate to similar levels

Toroidal domain length qualitatively changes energy loss process during pedestal collapse

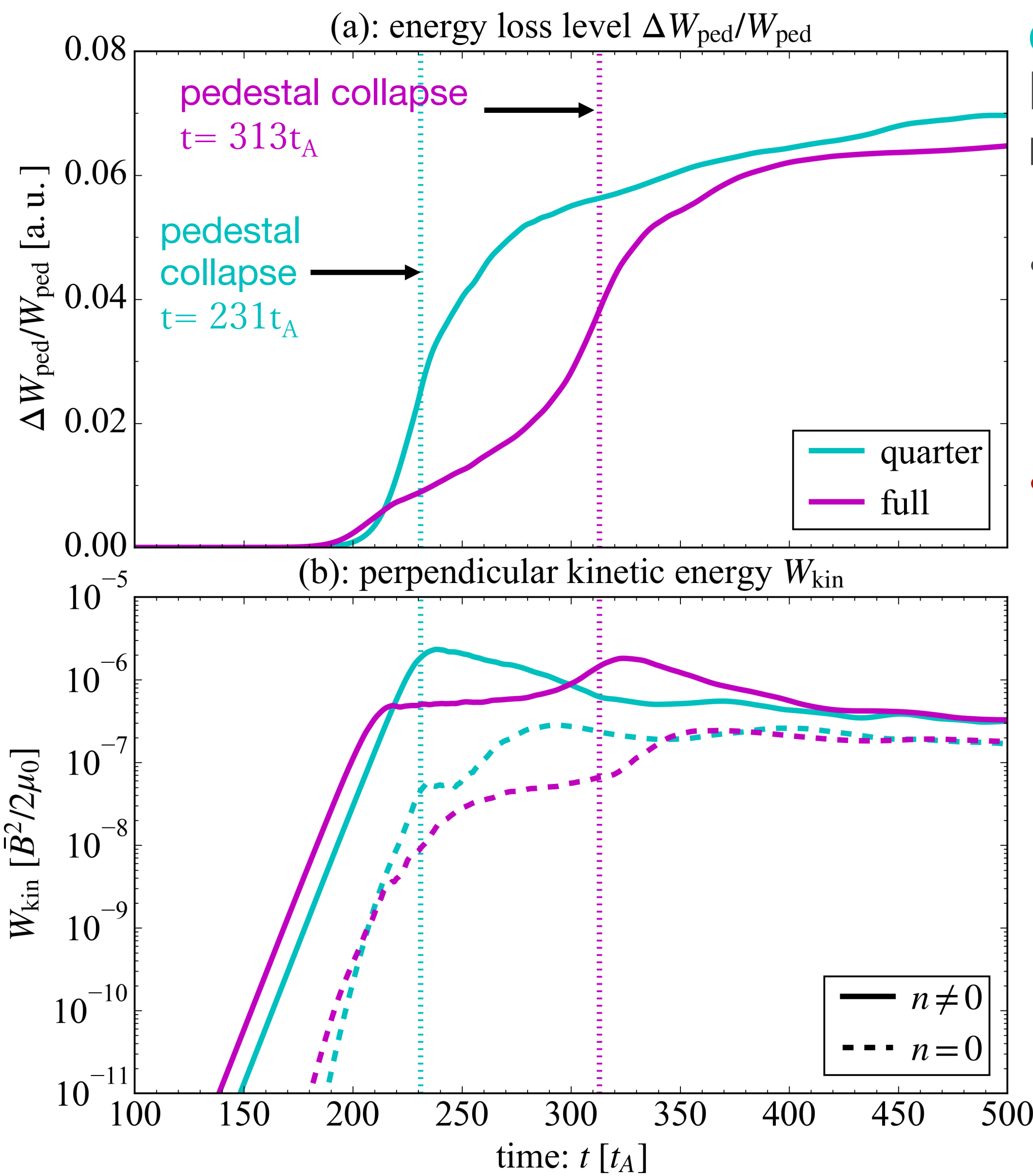

quarter and full toru run with Nx=1028, Ny=128, Nz= 64 or 256, n_{2Dmax}=4, n_{1Dmax}=80

- Resultant energy loss and n=0 and n≠0 amplitude of kinetic energy saturate to similar levels
- There are qualitative difference during pedestal collapse.

Initially unstable modes directly trigger the pedestal collapse and then n=0 & low-n modes are excited in quarter torus

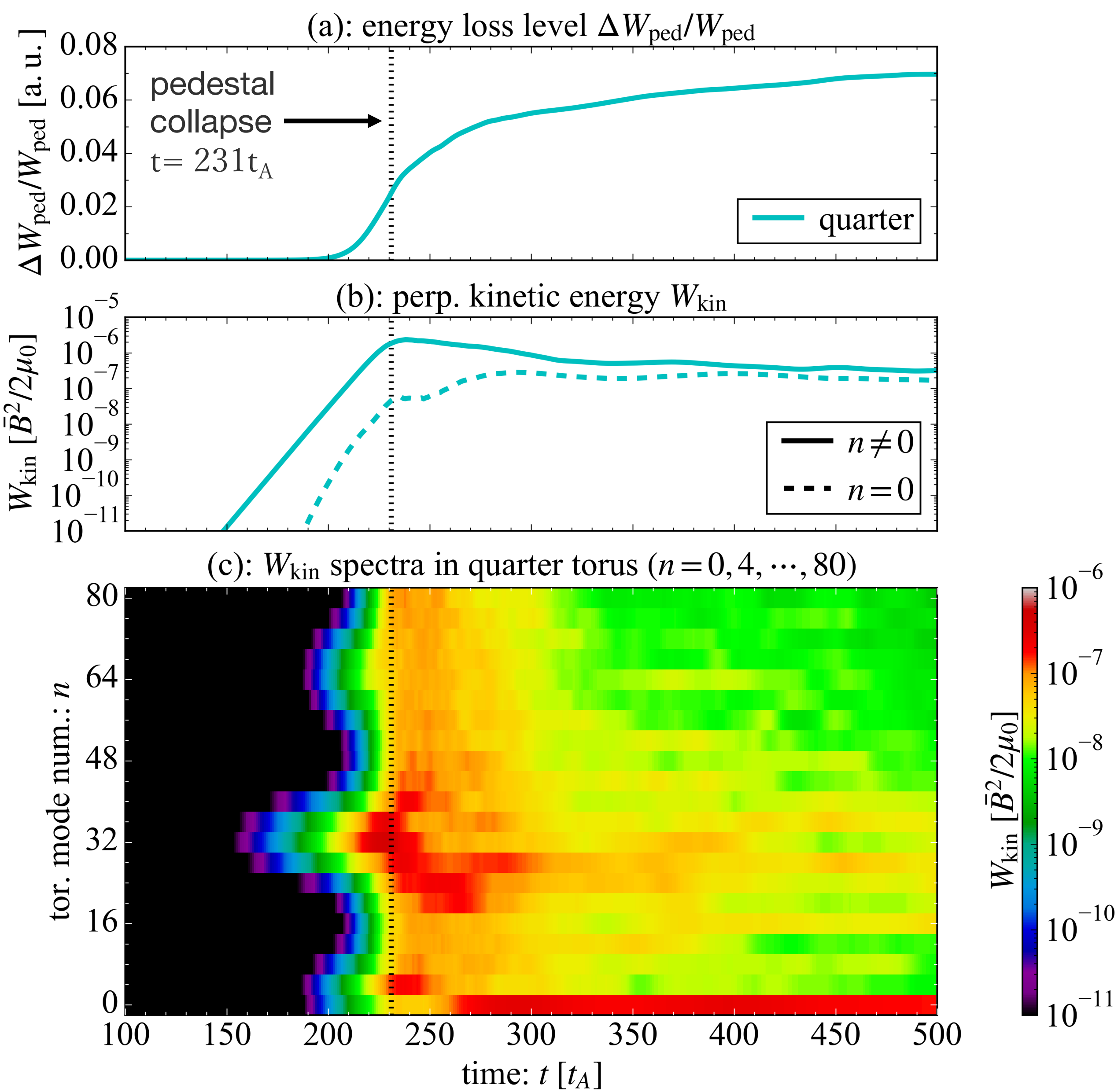

n=0 and low-n modes are excited before the collapse and the collapse is triggered by downshifted modes in full torus

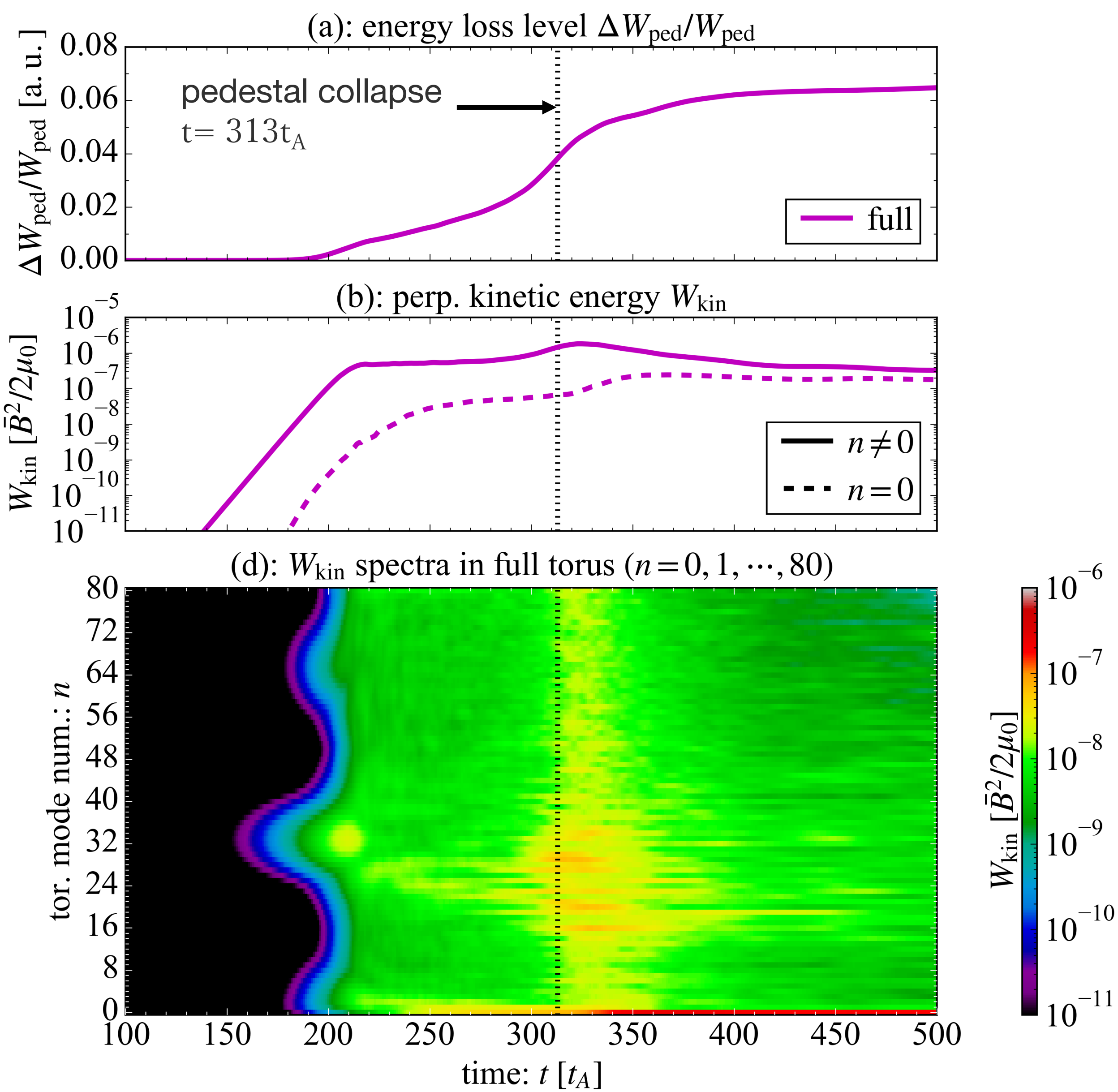

n=0 and low-n modes are excited before the collapse and the collapse is triggered by down-shifted modes in full torus

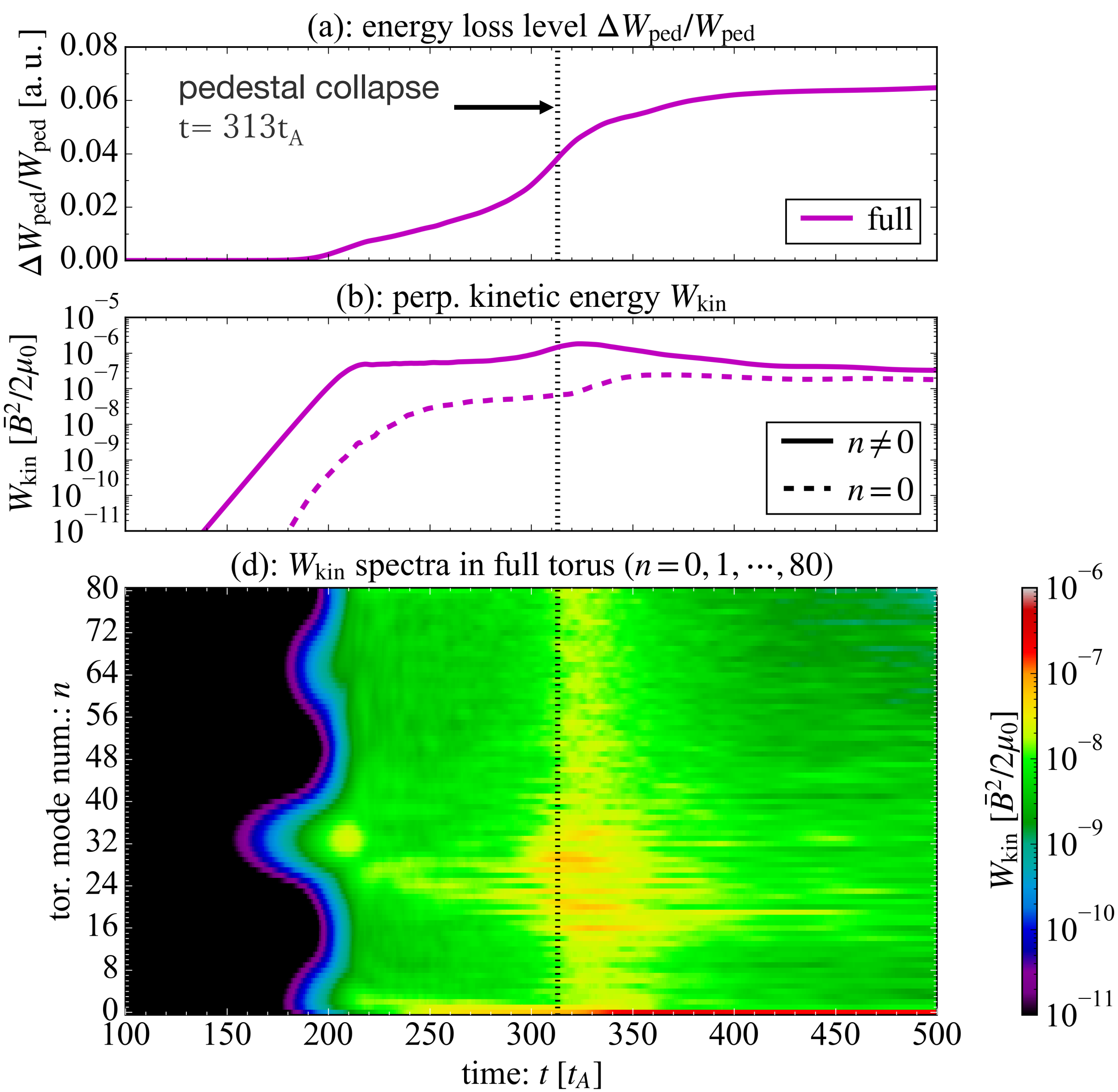

The observation of collapse delay in full torus is qualitatively consistent with the stabilization by nonlinear mode couplings [Xi+ PRL'14]

n=1 global mode is nonlinearly excited and coexists with fine-scale turbulence during the pedestal collapse in full torus case

(a): $n\neq0$ electrostatic potential during pedestal collapse($t=330t_A$)

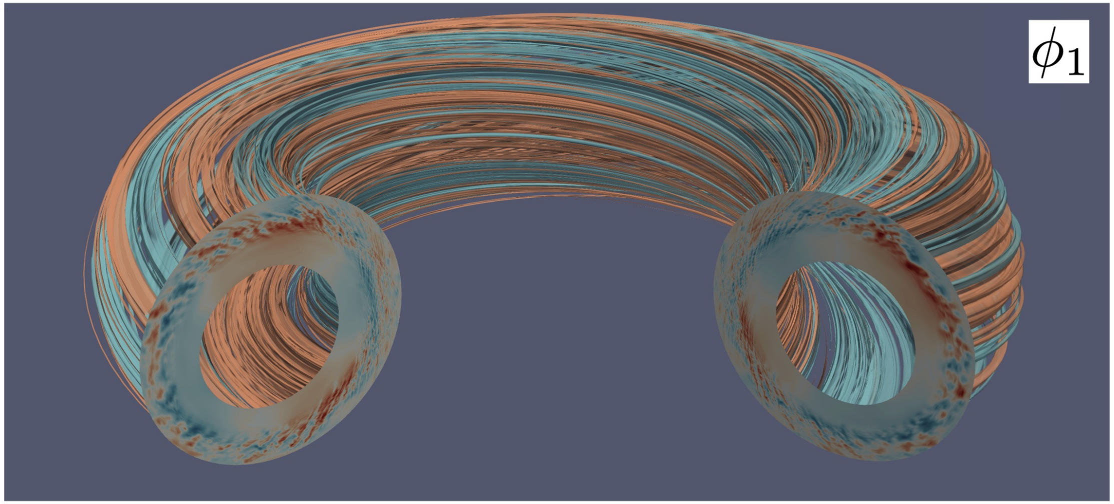

n=1 global mode is nonlinearly excited and coexists with fine-scale turbulence during the pedestal collapse in full torus case

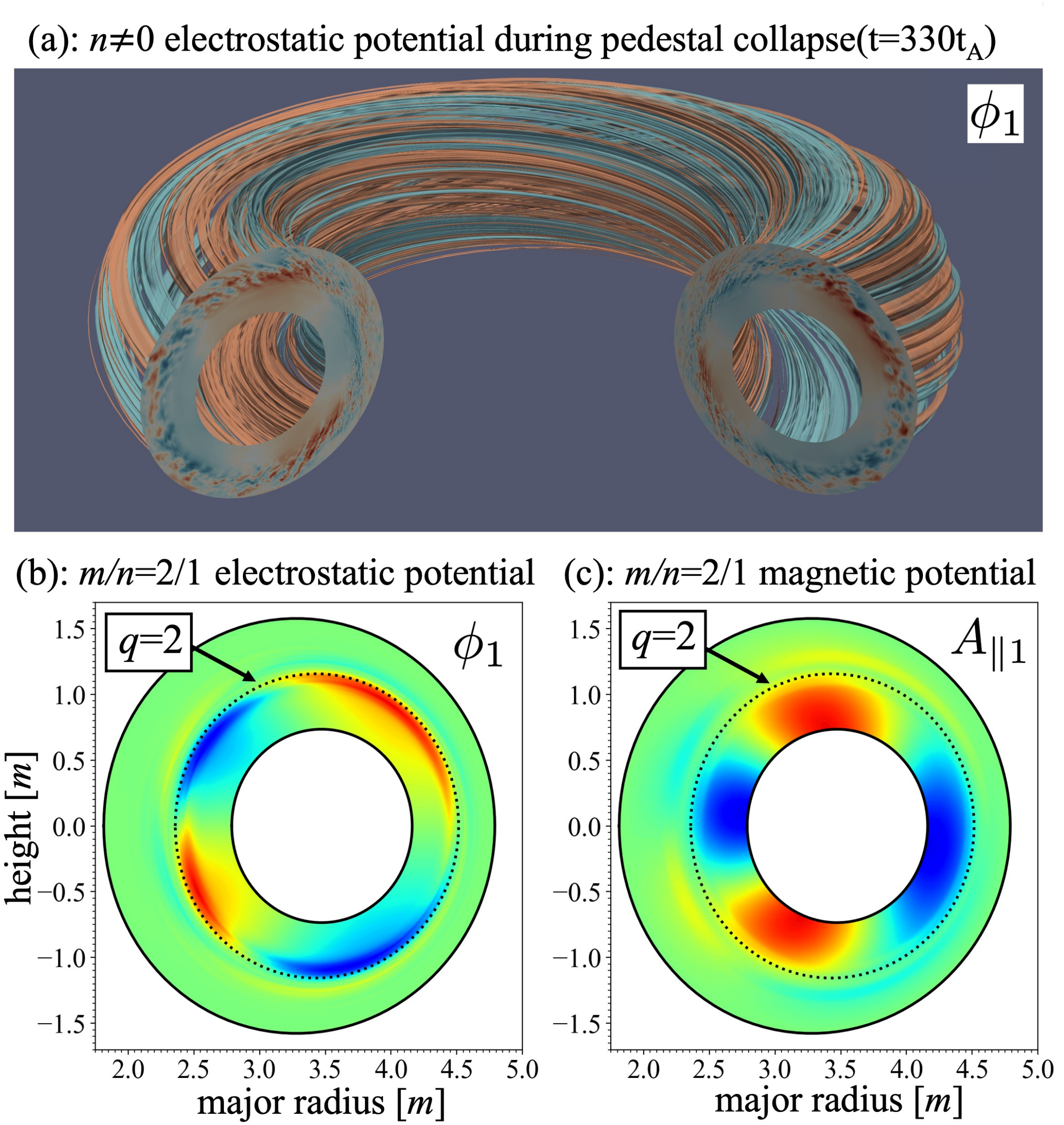

Global n=1 structure has m/n=2/1 tearing parity

Outline

- Introduction
- BOUT++ coordinate systems and hybrid field solver developed for full annular tokamak edge simulation
- Pedestal collapse with resistive drift-ballooning mode (RDBM) turbulence in full annular torus with shifted circular cross section
  - ➢ Scan of the maximum toroidal mode number solved by 2D field solver against pedestal collapse
  - ➢ Impact of truncated toroidal domain on energy loss process
  - ➢ Nonlinear generation on=1 global mode during pedestal collapse
- Summary

Summary

- **BOUT++ has been extended for full annular tokamak edge simulations by hybrid field solver, which covers n=0, low-n, moderate-n and high-n modes**
  - ➢ A key improvement for more self-consistent simulations of low-n mode relevant edge MHD and turbulence physics (type-I ELM, ELM control by RMPs, turbulence with RMPs, etc..)

- **Full annular pedestal collapse simulation has been carried out and has been compared with that with the quarter torus domain**
  - ➢ The truncated toroidal domain can qualitatively change the energy loss process during the pedestal collapse
  - ➢ Interplay between m/n=2/1 tearing like global structure and high-n fine-scale turbulence is observed during the pedestal collapse in the full torus case

- **On-going works**
  - ➢ Benchmark of 2D field solver against low-n modes
  - ➢ Full annular pedestal collapse simulation in single-null diverted geometry

Spatiotemporal structure of n=0 flow shear, low-n and high-n fluctuations

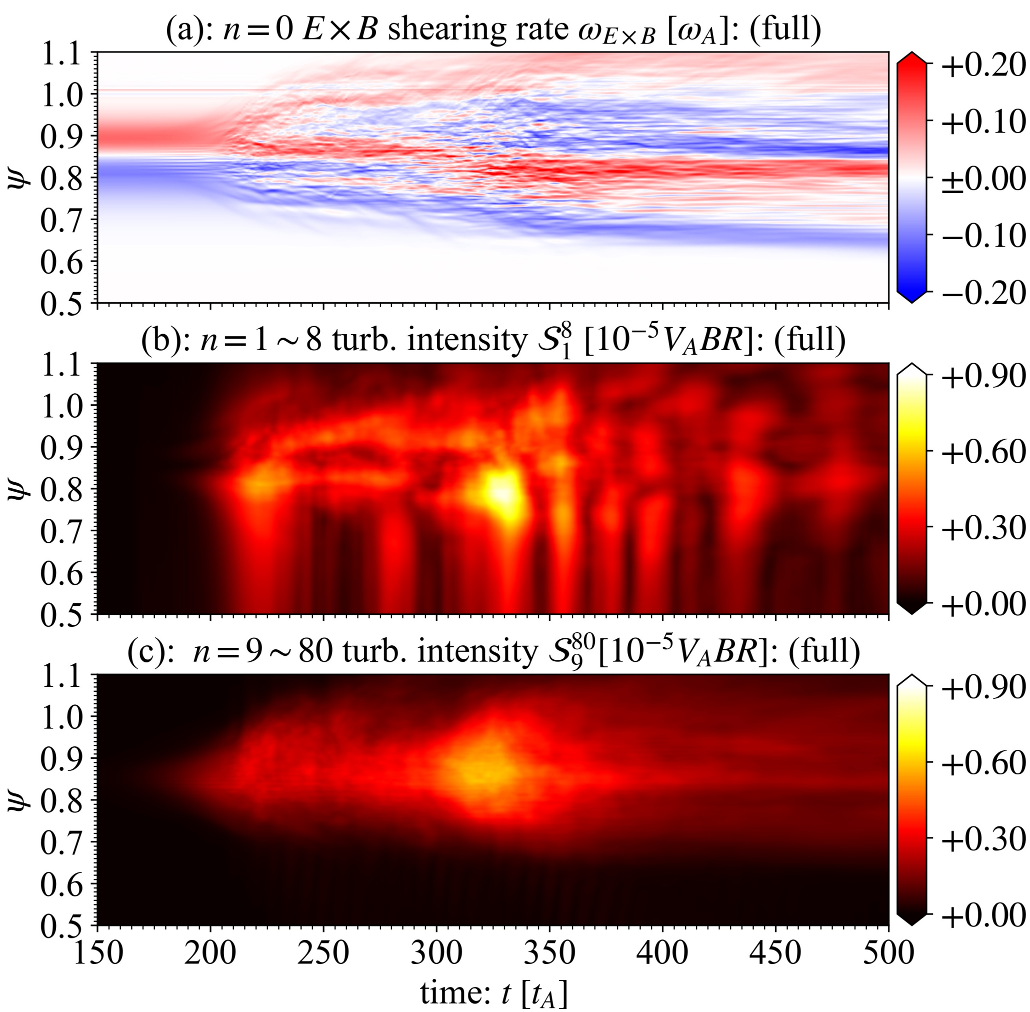

- Fine-scale zonal flow is generated by nonlinear couplings between high-n modes (t~200tA)
- Meso-scale zonal flow is then generated when low-n fluctuations are excited by nonlinear couplings between high-n modes (t=200tA~300tA)
- Large-scale mean flow is generated during pedestal collapse (t >330tA)
- Low-n fluctuations has radially elongated structure compared with high-n fluctuations

Details of generation mechanism of n=0 flow, those of interplay between n=0, low-n, and high-n modes are under investigation

Simulation setup for verification test of 2D field solver against IBM instability

Linearized 3-field IBM model

$$
\begin{aligned}
\frac{\partial U_1}{\partial t} &= -B_0\partial_\parallel\left(\frac{J_{\parallel 1}}{B_0}\right) + B_0\left[A_{\parallel 1}, \frac{J_{\parallel 0}}{B_0}\right] + \mathcal{K}(P_1),\\
\frac{\partial A_1}{\partial t} &= -\partial_\parallel \phi_1,\\
\frac{\partial P_1}{\partial t} &= -[\phi_1, P_0]\\
U_1 &= \nabla\cdot\left(\frac{n_{i0}}{B_0^2}\nabla_\perp\phi_1\right) = \frac{n_{i0}}{B_0^2}\nabla_\perp^2\phi_1 + \nabla\left(\frac{n_{i0}}{B_0^2}\right)\cdot\nabla_\perp\phi_1,\\
J_{\parallel 1} &= \nabla_\perp^2 A_{\parallel 1},\\
\partial_\parallel f &= \boldsymbol{b}_0\cdot\nabla f,\quad [f,g] = \frac{\boldsymbol{b}_0\times\nabla_\perp f\cdot\nabla_\perp g}{B_0},\quad \mathcal{K}(f) = \frac{\boldsymbol{b}_0\times\boldsymbol{\kappa}_0\cdot\nabla f}{B_0}
\end{aligned}
$$

- Normalized with poloidal Alfven units with R=3[m], B=2[T], n_i=10^{19} [m^{-3}], deuterium mass [Dudson CPC'09]
- Original BOUT++ employs flute-ordering in
  - ❖ Field solver for electrostatic potential

$$\left(\nabla_\perp^2 + B_0^2\nabla\frac{1}{B_0^2}\cdot\nabla_\perp\right)\phi_1 = B_0^2 U_1$$

  - ❖ Laplacian operator for parallel current density

$$J_1 = \nabla_\perp^2 A_{\parallel 1}$$

IBM strongly unstable shifted circular equilibrium [Snyder PoP'02, Wilson PoP'02]

- Equilibrium used in cross-code benchmarks [Dudson CPC'09, PPCF'11, Ferraro PoP'10 etc…]
- IBM growth rates are calculated with 1D & 2D solver in $1/N$-th annular wedge domains for n=N mode

	Nx	Ny	Nz	z-length
1D field solver & Laplacian	512	64	32	$2\pi/N$
2D field solver & Laplacian	512	512	32	$2\pi/N$

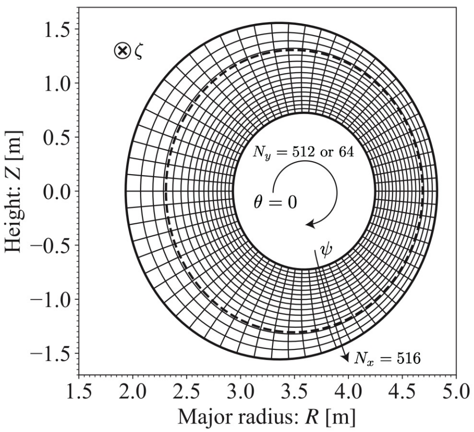

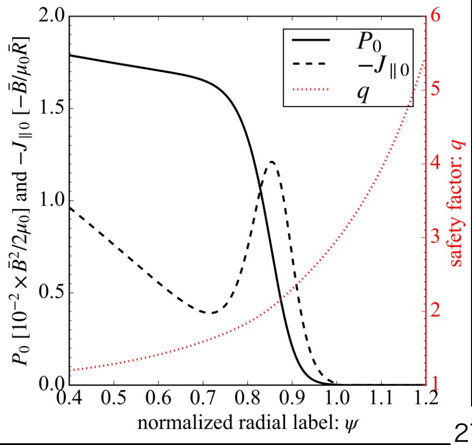

2D field solver can get n=20 IBM but flute-ordering has impact on low-n regime

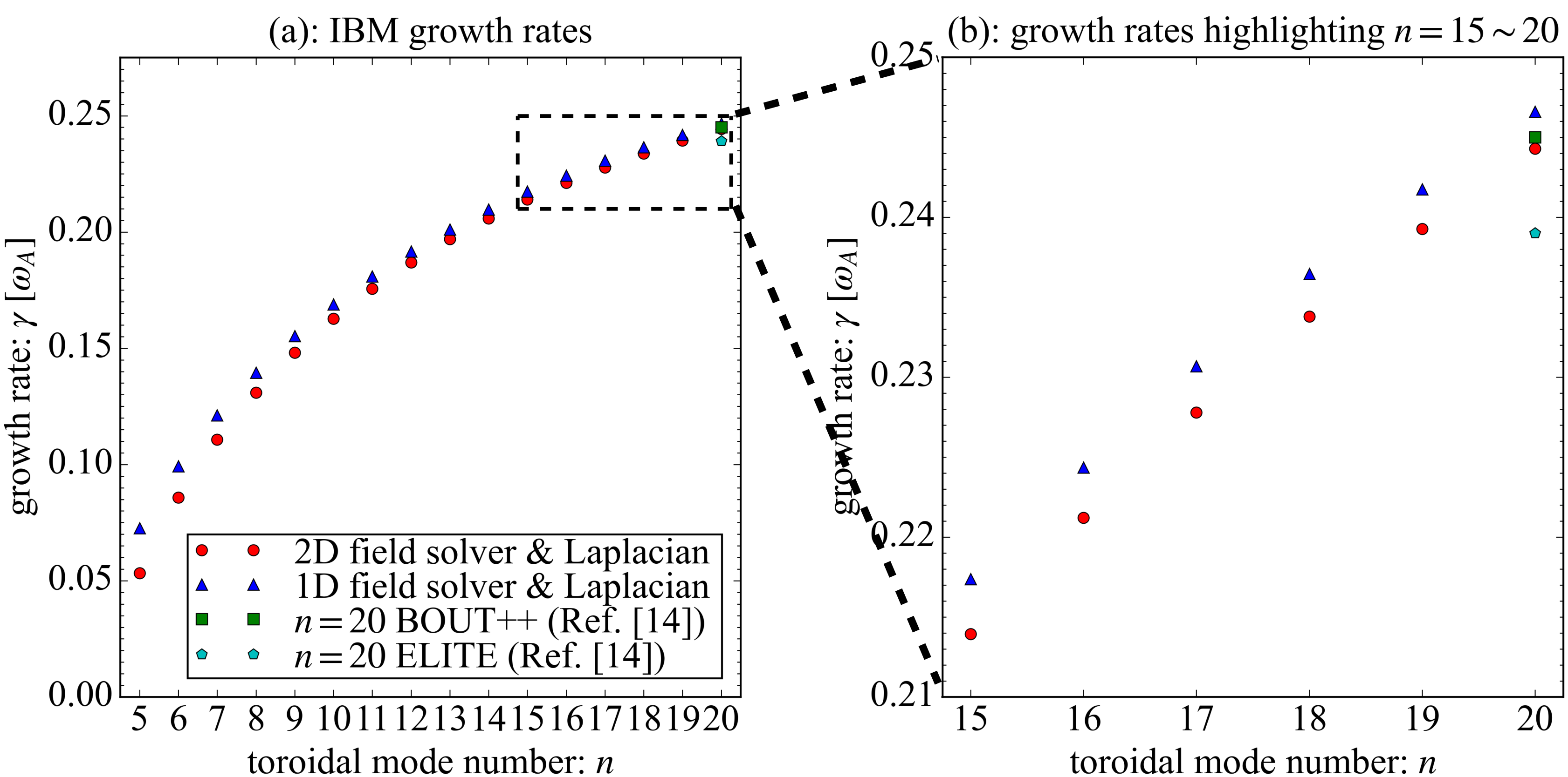

- n=20 IBM growth rate by 2D field solver shows good agreement with the previous work [Ref. [14] Dudson CPC'09]
- The difference between growth rates by 2D solver and those by 1D solver becomes larger for lower-n modes

➡ Qualitatively consistent with the expected flute-ordering correction of O(1/n) [Connor PRSA'79]

flux-surface & field-aligned coords. are used with shifted metric

quarter torus domain: (ψ,θ,ζ)

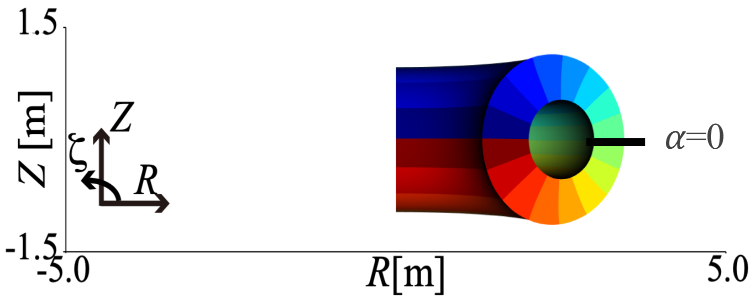

- Need fine pol.(θ) grids for parallel difference $m_{\mathrm{res}} = nq$
- No cell deformation by magnetic shear

Used for (ζ,ψ)-difference

flux-surface & field-aligned coords. are used with shifted metric

quarter torus domain: (ψ,θ,ζ)

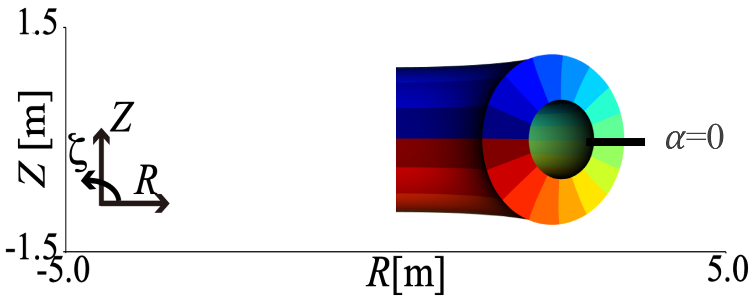

- Need fine pol.(θ) grids for parallel difference $m_{\rm res}= nq$
- No cell deformation by magnetic shear

Used for (ζ,ψ)-difference

shift: $z=\zeta-\alpha$

$$x = \psi - \psi_0$$
$$y = \theta$$
$$z = \zeta - \alpha$$
$$\alpha = \int_{\pi}^{\theta} \frac{B^{\zeta}}{B^{\theta}} d\theta$$

shift: $\zeta = z+\alpha$

quarter torus domain: (x,y,z)

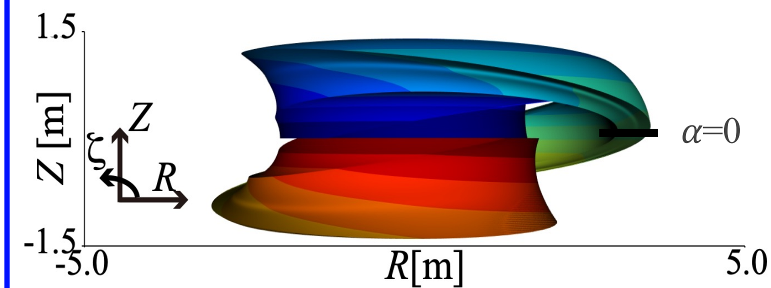

- Need only coarse para.(y) grids for parallel difference
- Radial difference is degraded by cell-deformation

Used for (y,z)-difference

flux-surface & **field-aligned** coords. are used with shifted metric

quarter torus domain: (ψ,θ,ζ)

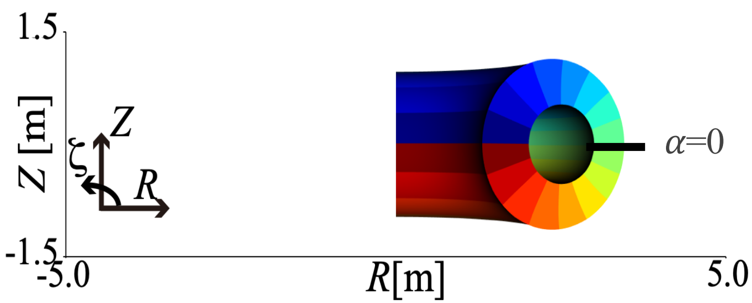

- Need fine pol.(θ) grids for parallel difference $m_{\mathrm{res}} = nq$
- No cell deformation by magnetic shear

Used for (ζ,ψ)-difference

shift: $z=\zeta-\alpha$

$$x = \psi - \psi_0$$
$$y = \theta$$
$$z = \zeta - \alpha$$
$$\alpha = \int_{\pi}^{\theta} \frac{B^{\zeta}}{B^{\theta}} d\theta$$

shift: $\zeta = z+\alpha$

quarter torus domain: (x,y,z)

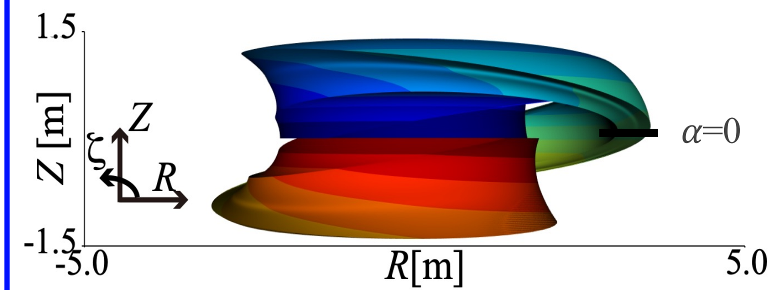

- Need only coarse para.(y) grids for parallel difference
- Radial difference is degraded by cell-deformation

Used for (y,z)-difference

- **Helmholtz Eq. of flow potential:** $\left(d\nabla_{\perp}^2 + \frac{1}{c}\nabla c \cdot \nabla_{\perp} + a\right) f(x,y,z) = h(x,y,z)$
  - Eq. for toroidal mode n in quasi-ballooning coords. has ψ- and y- derivatives

$$d\left[L_{\mathrm{qb}}^{10}\frac{\partial}{\partial\psi} + L_{\mathrm{qb}}^{11}\frac{\partial^2}{\partial\psi^2} + \left(L_{\mathrm{qb}}^{20} + inL_{\mathrm{qb}}^{23}\right)\frac{\partial}{\partial y} + L_{\mathrm{qb}}^{22}\frac{\partial^2}{\partial y^2} + inL_{\mathrm{qb}}^{30} - n^2L_{\mathrm{qb}}^{33}\right]F + \frac{1}{c}\left(G_{\mathrm{qb}}^{1}\frac{\partial c}{\partial\psi}\frac{\partial}{\partial\psi} + G_{\mathrm{qb}}^{2}\frac{\partial c}{\partial y}\frac{\partial}{\partial y} + inG_{\mathrm{qb}}^{3}\frac{\partial c}{\partial y}\right)F + aF = H$$

$$\longrightarrow d\left(L_{\mathrm{qb}}^{10}\frac{\partial}{\partial\psi} + L_{\mathrm{qb}}^{11}\frac{\partial^2}{\partial\psi^2} + inL_{\mathrm{qb}}^{30} - n^2L_{\mathrm{qb}}^{33}\right)F(\psi|\theta,n) + \frac{1}{c}\left(G_{\mathrm{qb}}^{1}\frac{\partial c}{\partial\psi}\frac{\partial}{\partial\psi} + inG_{\mathrm{qb}}^{3}\frac{\partial c}{\partial y}\right)F(\psi|\theta,n) + aF(\psi|\theta,n) = H(\psi|\theta,n)$$

Flute-ordering reduces Eq. to 1D (ψ-dir) but can give numerical instability on low-n